Photoinduced electron transfer and energy transfer processes in a new BODIPY-C 60 Dyad

Thu-Trang Tran, Jad Rabah, Minh-Huong Ha-Thi, Emmanuel Allard, Stanislaw Nizinski, Gotard Burdzinski, Stéphane Aloïse, Hélène Fensterbank, Krystyna Baczko, Houssein Nasrallah, et al.

Light-induced electron transfer and energy transfer processes in a new BODIPY-C_{60} Dyad

Thu-Trang Tran,[†,§] Jad Rabah,[‡] Minh-Huong Ha-Thi,[†] Emmanuel Allard,[‡]* Stanislaw Nizinski,[#] Gotard Burdzinski,[#] Stéphane Aloïse,[$] Hélène Fensterbank,[‡] Krystyna Baczko,[‡] Houssein Nasrallah,[‡] Anne Vallée,[‡] Gilles Clavier,[⊥] Fabien Miomandre,[⊥] Thomas Pino,[†] and Rachel Méallet-Renault[†]**

[†]Institut des Sciences Moléculaires d'Orsay, CNRS, Univ. Paris-Sud, Université Paris-Saclay, 91405 Orsay Cedex, France

[‡]Institut Lavoisier de Versailles, UMR 8180, Université de Versailles Saint-Quentin-en-Yvelines, Université Paris-Saclay, 78035 Versailles Cedex, France

[#]Adam Mickiewicz Univ in Poznan, Fac Phys, Quantum Elect Lab, PL-61614 Poznan, Poland

[⊥]PPSM, CNRS-ENS Paris Saclay, 61 Avenue Président Wilson, 94235 CACHAN, France

[$]Univ Lille, CNRS, UMR 8516, LASIR, Lab Spectrochim Infrarouge & Raman, F-59000 Lille, France

§ Faculty of Physics and Technology, Thai Nguyen University of Science, Thai Nguyen, Vietnam

KEYWORDS: Electron transfer, energy transfer, BODIPY, fullerene, dyad, transient absorption.

ABSTRACT: A new donor−acceptor dyad composed of a BODIPY (4,4′-difluoro-4-bora-3a,4a-diaza-s-indacene) donor and a fullerene C60 acceptor has been synthesized and characterized. This derivative has been prepared using a clickable fullerene building block that bears an alkyne moiety and a maleimide unit. The post-functionalization of the maleimide group by a BODIPY thiol leads to a BODIPY-C60 dyad, leaving the alkyne moiety for further functional arrangement. On the basis of the combination of semi-empirical and density functional theory (DFT) calculations, spectroelectrochemical experiments, and steady-state and time-resolved spectroscopies, the photophysical properties of this new BODIPY-C60 dyad were thoroughly studied. By using semi-empirical calculations, the equilibrium of three conformations of the BODIPY-C60 dyad has been deduced, and their molecular orbital structures have been analyzed using DFT calculations. Two short fluorescence lifetimes were attributed to two extended conformers displaying variable donor−acceptor distances (17.5 and 20.0 Å). Additionally, the driving force for photoinduced electron transfer from the singlet excited state of BODIPY to the C60 moiety was calculated using redox potentials determined with electrochemical studies. Spectroelectrochemical measurements were also carried out to investigate the absorption profiles of radicals in the BODIPY-C60 dyad in order to assign the transient species in pump−probe experiments. Under selective photoexcitation of the BODIPY moiety, occurrences of both energy and electron transfers were demonstrated for the dyad by femtosecond and nanosecond transient absorption spectroscopies. Photoinduced electron transfer occurs in the folded conformer, while energy transfer is observed in extended conformers.

1. Introduction

helicalThe association of donor and acceptor in dyads (and polyads) has significantly contributed to the development of many light-harvesting materials for organic electronics.[1-21] These systems

are able to undergo electron transfer and/or energy transfer due to photo-excitation either of the donor or acceptor moiety. Studies on these light-induced processes, and more specifically electron transfer, are of prime importance not only from a fundamental point of view but also for practical applications.[2-21] Indeed, conversion of solar light energy into electricity in photovoltaics or to chemical energy (solar fuel) through photocatalytic processes invariably starts with photoinduced electron transfer (PET).[22] Consequently, a huge number of donor-acceptor conjugates have been designed and light-induced electron transfer and/or energy transfer events in solution have been probed.[1-21] Among the different acceptors, fullerene C_{60} is probably the most attractive one due to its outstanding properties including good electron acceptor capability, a high degree of charge delocalization within the π-extended conjugation and small reorganization energies in electron transfer processes.[20, 23] Regarding the chromophores used both as light-harvester and electron donor, 4,4'-Difluoro-4-bora-3a,4a-diaza-s-indacenes (referred to as BODIPYs) have recently gained more attention in the design of donor-C_{60} conjugates.[24-39] Indeed, BODIPYs (BDPs) are chemically stable and display remarkable photophysical properties, including high absorption coefficients and emission quantum yields. Another remarkable feature relies on the ease of functionalization of the BDP core, allowing to tune its spectral and electrochemical properties.[40] In many examples, it was shown that the PET in these BDP-C_{60} assemblies was the main pathway leading to charge separated states,[25-26, 28, 30-36, 38] whereas energy transfer appeared as a competitive process in a few cases.[24, 27]

The occurrence of this PET in these BDP-fullerene systems observed in solution could also be exploited in the construction of photocurrent generating photoelectrochemical cells. These molecular photovoltaic devices have already been prepared from self-assembled monolayers (SAMs) of donor-fullerene systems on gold surfaces, mainly with porphyrin-fullerene

conjugates.[41-42] However, the existence of energy transfer of the excited state of the chromophores by the metallic surface has appeared as a limiting factor for the photocurrent generation.[2, 41] In this context, it was recently proposed that The association of a donor and acceptor in dyads (and polyads) has significantly contributed to the development of many light-harvesting materials for organic electronics.(1−22) These systems are able to undergo electron transfer and/or energy transfer due to photoexcitation of either the donor or acceptor moiety. Studies on these light-induced processes and, more specifically, electron transfer, are of prime importance not only from a fundamental point of view but also for practical applications.(2−22) Indeed, conversion of solar light energy into electricity in photovoltaics or to chemical energy (solar fuel) through photocatalytic processes invariably starts with photoinduced electron transfer (PET).(23) Consequently, a huge number of donor–acceptor conjugates have been designed and light-induced electron transfer and/or energy transfer events in solution have been probed.(1−22) Among the different acceptors, fullerene C60 is probably the most attractive one due to its outstanding properties including good electron acceptor capability, a high degree of charge delocalization within the π-extended conjugation, and small reorganization energies in electron transfer processes.(20,24) Regarding the chromophores used both as light-harvesters and electron donors, 4,4′-difluoro-4-bora-3a,4a-diaza-s-indacenes (referred to as BODIPYs) have recently gained more attention in the design of donor-C60 conjugates.(25−40) Indeed, BODIPYs are chemically stable and display remarkable photophysical properties, including high absorption coefficients and emission quantum yields. Another important feature relies on the ease of functionalization of the BODIPY core, allowing to tune its spectral and electrochemical properties.(41) In many examples, it has been shown that the PET in these BODIPY-C60 assemblies was the main pathway leading

to charge-separated states,(26,27,29,31−37,39) whereas energy transfer appeared as a competitive process in a few cases.(25,28)

The occurrence of this PET in these BODIPY-fullerene systems observed in solution could also be exploited in the construction of photocurrent-generating photoelectrochemical cells. These molecular photovoltaic devices have already been prepared from self-assembled monolayers (SAMs) of donor-fullerene systems on gold surfaces, mainly with porphyrin-fullerene conjugates.(42,43) However, the existence of energy transfer from the excited state of the chromophores to the metallic surface has appeared as a limiting factor for photocurrent generation.(2,42) In this context, it was recently proposed that helical peptide could be used as a spacer between the chromophore and the gold surface. The rigid helical conformation adopted by the peptide keeps the chromophore away from the surface and thus prevents (or limits) the quenching of the chromophore excited state.(44,45) Another remarkable feature of the helical peptide is related to its good electron mediator ability compared to an alkyl chain.(44,45) Thus, promising results have been recently obtained with peptide-based SAMs functionalized with electroactive and/or photoactive probes in the construction of devices for photo-energy conversion applications.(45−47)

Consequently, we are interested in the synthesis of a BODIPY-C60 dyad that could be associated with a helical peptide. The resulting BODIPY-C60-peptide assembly could then be immobilized on surfaces to develop photoelectrochemical devices. To accomplish this goal, we have to first address the synthesis and the photophysical characterization of a BODIPY-C60 dyad that could be used as a building block in the design of dyad-terminated helical peptides (Figure 1).

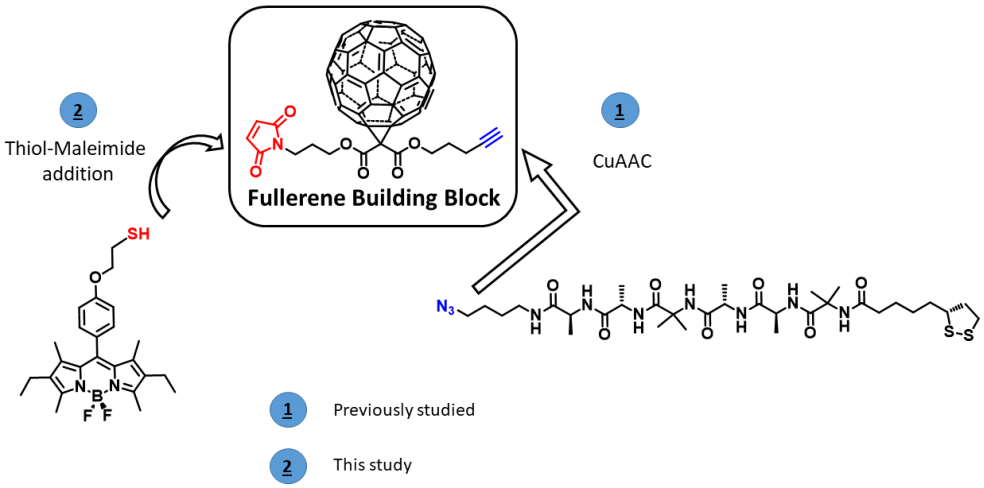

Figure 1. Scheme of "clickable" fullerene with two different reactive centers: an alkyne moiety (in blue) and a maleimide unit (in red). Steps 1 and 2 indicate the sequential orthogonal transformations based on copper(I)-catalyzed alkyne-azide cycloaddition (CuAAC) and thiol-maleimide "click" reactions.

Herein, we present the synthesis of a BODIPY-C60 dyad obtained from a "clickable fullerene" and BODIPY derivatives. Previously reported BODIPY-C60 dyads were prepared by direct functionalization of C60 in the final step.(26−29,31,32,34−38,40) What makes our system different is the use of the "clickable" fullerene building block that bears two different reactive centers: an alkyne moiety on one side and a maleimide unit on the other side (Figure 1). This derivative can be easily functionalized using sequential orthogonal transformations based on copper(I)-catalyzed alkyne-azide cycloaddition (CuAAC) and thiol-maleimide "click" reactions, as we have previously demonstrated.(48,49) In the present study, the fullerene building block is functionalized with a BODIPY thiol, leaving the alkyne moiety available for further functional arrangement with a peptide azide through the use of a CuAAC reaction.(50) In this contribution, the photoinduced processes in this BODIPY-C60 dyad were investigated, thanks to the

combination of computational studies, spectroelectrochemical experiments, and steady-state and time-resolved spectroscopy techniques.

2. Experimental section

2.1 Synthesis

2.1.1 General Methods

All reagents were used directly without further purification. The purity of fullerene C60 was 99.5+%. Dichloromethane (DCM) was dried on CaCl2 and distilled over CaH2 prior to use. Toluene was distilled over NaH prior to use. All other solvents were used as received. Column chromatography was performed using silica gel 60 (0.040–0.063 mm). Thin-layer chromatography (TLC) was performed on aluminum sheets coated with silica gel 60 F254. NMR spectra were determined in CDCl3, and chemical shifts were referenced to this internal solvent (7.26 ppm for 1H and 77.16 ppm for 13C). High-resolution electrospray ionization mass spectra were obtained with a Qtof analyzer type.

2.1.2 Synthesis of 1

Fullerene-maleimide **1** was prepared in five steps according to a previously published procedure.[48]

2.1.3 Synthesis of 2

In a round bottomed flask, 50mg of protected fullerene-maleimide **1** was introduced with 3 mL of dried toluene. The reaction mixture was stirred overnight at 110°C and evaporated to dryness. Purification of the black residue by column chromatography (SiO_2, DCM) gave 44mg of a black solid in 94% yield. 1H NMR (300MHz, $CDCl_3$) δ 2.03 (t, 1H, J = 2.6 Hz, H_a), 2.05-2.13 (m, 2H, H_d), 2.13-2.21 (m, 2H, H_j), 2.42 (dt, 2H, J = 6.9 Hz, J = 2.6 Hz, H_c), 3.75 (t, 2H, J = 6.8 Hz, H_k), 4.52 (t, 2H, J = 6.2 Hz, H_i), 4.65 (t, 2H, J = 6.2 Hz, He), 6.75 (s, 2H, H_m); ^{13}C NMR (75 MHz,

$CDCl_3$) δ 15.4 (C_c), 27.5 (C_d), 27.9 (C_j), 35.0 (C_k), 64.9 (C_i), 66.0 (C_e), 69.8 (C_a), 71.6 ($_{Csp3\ C60}$), 82.7 (C_b), 134.4 (C_m), [139.0, 139.3, 141.2, 142.1, 142.4, 143.1, 143.2, 143.22, 144.0, 144.76, 144.79, 144.81, 144.84, 145.1, 145.2, 145.22, 145.3, 145.4, 145.42 (Csp2 C60)], 163.6 (C_f, C_h), 170.8 (C_l); HRMS (ESI+) m/z calcd for $C_{75}H_{15}NO_6Na$: 1048.0797 [M + Na^+], found 1048.0863.

2.1.4 Synthesis of 3

In a three-necked flask, 4-(2-bromoethoxy)benzaldehyde (0.66g, 2.87mmol) was dissolved in anhydrous DCM (50 mL), argon was bubbled through the solution for 10 min. To this oxygen-free solution were added successively kryptopyrrole (0.9ml, 6.60mmol) and trifluoroacetic acid (0.6mL). The reaction mixture was stirred for 2 hours and chloranil (0.71g, 2.87mmol) was then added, the reaction was further stirred for 5 minutes. N,N-Diisopropylethylamine (DIPEA, 3.5mL, 20.1mmol) was then added to the mixture that was left to stir for 15 minutes. Boron trifluoride etherate (3.9mL, 31.6mmol) was finally introduced to the reaction. The resulting solution was stirred at room temperature for 2 hours and evaporated to dryness. Purification of the black-red residue by column chromatography (SiO_2, EP/DCM 1:2) gave 625mg of a red solid in 44% yield. ^{1}H NMR (300MHz, $CDCl_3$) δ 0.98 (t, 6H, J = 7.6 Hz, H_B), 1.32 (s, 6H, H_D), 2.30 (q, 4H, J = 7.6 Hz, H_C) ; 2.52 (s, 6H, H_A), 3.70 (t, 2H, J = 6.2 Hz, H_H), 4.36 (t, 2H, J = 6.2 Hz, H_G), 7.02 (d, 2H, J = 8.7 Hz, H_F or H_E), 7.19 (d, 2H, J = 8.6 Hz, H_F or H_E); ^{13}C NMR (75 MHz, $CDCl_3$) δ 12.0 (C_D), 12.6 (C_A), 14.8 (C_B), 17.2 (C_C), 29.1 (C_H), 68.1 (C_G), 115.4 (C_E or C_F), 128.9, 129.8 (C_E or C_F), 131.1, 132.9, 138.5, 153.8, 158.7; ^{19}F NMR (188 MHz, $CDCl_3$) δ -145.81 (q, J = 33.2 Hz); 11B RMN (96 MHz, $CDCl_3$) δ 2.25 (t, J = 33.5 Hz); HRMS (ESI+) m/z calcd for $C_{25}H_{31}BBrF_2N_2O$: 505.1660 $[M+H]^+$, found 505.1665.

2.1.5 Synthesis of 4

To a two-necked flask was added BDP-bromide **3** (590mg, 1.18mmol) and potassium thioacetate (280mg, 2.47mmol) in anhydrous acetone (25mL). The reaction mixture was stirred overnight under reflux at 60°C. The crude product was taken up in DCM and washed with water and finally dried over $MgSO_4$. Purification of the crude product by column chromatography (SiO_2, DCM/EP 1:1.3 then 1:1) gave 475mg of a red solid in 81% yield. ^{1}H NMR (300 MHz, $CDCl_3$) δ 0.98 (t, 6H, J = 7.5 Hz, H_B), 1.32 (s, 6H, H_D), 2.30 (q, 4H, J = 7.5 Hz, H_C), 2.40 (s, 3H, H_I); 2.52 (s, 6H, H_A), 3.32 (t, 2H, J = 6.5 Hz, H_H), 4.15 (t, 2H, J = 6.2 Hz, H_G), 7.01 (d, 2H, J = 8.6 Hz, H_F or H_E) ; 7.17 (d, 2H, J = 8.6 Hz, H_F or H_E); ^{13}C NMR (75 MHz, $CDCl_3$) δ 12.0 (C_D), 12.6 (C_A), 14.8 (C_B), 17.2 (C_C), 28.5 (C_H), 30.8 (C_I), 66.7 (C_G), 115.2 (C_F), 128.5, 129.7 (C_E), 131.3, 132.8, 138.5, 140.2, 153.7, 158.9, 195.5 (C=O); ^{19}F NMR (188 MHz, $CDCl_3$) δ -145.76 (q, J = 35.0 Hz); ^{11}B RMN (96 MHz, $CDCl_3$) δ 2.24 (t, J = 35.0 Hz); HRMS (ESI+) m/z calcd for $C_{27}H_{33}BF_2N_2O_2S$: 497.2360 [$M^{+\bullet}$], found 497.2361.

2.1.6 Synthesis of 6

In a round bottomed flask, a BDP-thioacetate **4** (80mg, 0.16 mmol) was dissolved in a mixture of dried MeOH/DCM (10mL:6 mL), argon was bubbled through the solution for 20 min. Potassium carbonate (22mg, 0.16mmol) was then added to this oxygen-free solution, and the resulting reaction mixture was stirred for 1 hour. Potassium carbonate was filtered and the solvent was evaporated under reduced pressure. Dried DCM (5mL) was then added to the solid, and argon was bubbled through the solution for 10 min. To this oxygen-free solution was added tributylphosphine (0.04mL, 0.16mmol). The resulting reaction mixture was stirred for 30 minutes at room temperature and evaporated to dryness. Purification of the crude product by column chromatography (SiO_2, DCM/EP: 3/1) gave 60mg of a red solid in 82% yield. ^{1}H NMR (300 MHz,

$CDCl_3$) δ 0.98 (t, 6H, J = 7.5 Hz, H_B), 1.33 (s, 6H, H_D), 1.74 (t, 1H, J = 8.5 Hz, H_I), 2.30 (q, 4H, J = 7.5 Hz, H_C), 2.53 (s, 6H, H_A), 2.96 (dt, 2H, J = 8.4Hz, J = 6.4Hz, H_H), 4.18 (t, 2H, J = 6.4Hz, H_G), 7.01 (d, 2H, J = 8.6Hz, H_E or H_F), 7.18 (d, 2H, J = 8.5Hz, H_E or H_F); ^{19}F NMR (282MHz, $CDCl_3$) δ -145.73 (q, J = 34.8Hz); ^{11}B RMN (96 MHz, $CDCl_3$) δ 2.25 (t, J = 35.1 Hz); HRMS (ESI+) m/z calcd for $C_{25}H_{31}BF_2N_2OS$:456.2218 [M + Na^+], found 456.2229.

2.1.7 Synthesis of the BDP-C_{60} Dyad

In a round bottomed flask, a BDP-thiol **6** (60mg, 0.13mmol) was dissolved in 10mL of dried DCM, argon was bubbled through the solution for 30 min. To this oxygen-free solution were added successively the fullerene-maleimide **2** (67mg, 0.065mmol) and 0.03mL (0.22mmol) of triethylamine. The reaction mixture was stirred overnight at room temperature under argon and evaporated to dryness. Purification of the crude product by column chromatography (SiO_2, DCM/Et_2O: 96/2) gave 83mg of a black solid in 87% yield. ^1H NMR (300 MHz, $CDCl_3$) δ 0.98 (t, 6H, J = 7.5 Hz, H_B), 1.32 (s, 6H, H_D), 2.04 (t, 1H, J = 2.6 Hz, H_a), 2.05 – 2.12 (m, 2H, H_d), 2.15-2.22 (m, 2H, H_j), 2.30 (q, 4H, J = 7.4 Hz, H_C), 2.42 (dt, 2H, J = 6.9 Hz, J = 2.6 Hz, H_c), 2.52 (s, 6H, H_A), 2.61 (dd, 1H, J = 18.8 Hz, J = 3.5 Hz, H_{m2}), 3.12-3.21 (m, 1H, H_{H2}), 3.29 (dd, 1H, J = 18.7Hz, J = 9.0Hz, H_{m1}), 3.43-3.50 (m, 1H, H_{H1}), 3.78 (dt, 2H, J = 6.7Hz, J = 2.4Hz, H_k), 4.04 (dd, 1H, J = 9.0Hz, J = 3.5Hz, H_n), 4.23-4.37 (m, 2H, H_G), 4.54 (m, 2H, H_i), 4.64 (t, 2H, J = 6.2Hz, H_e), 7.01 (d, 2H, J = 8.6 Hz, H_E or H_F), 7.17 (d, 2H, J = 8.6 Hz, H_E or H_F); ^{13}C NMR (75 MHz, $CDCl_3$): δ 12.1 (C_D), 12.6 (C_A), 14.8 (C_B), 15.4 (C_d), 17.2 (C_C), 27.1, 27.5, 31.3, 36.2, 36.5, 39.5 (C_n), 52.1 (C_g), 65.0 (C_i), 66.0 (C_e), 67.7, 69.9 (C_a), 71.6 ($C_{sp3\ C60}$), 82.6 (C_b), 115.2 (C_E or C_F), 128.7 ($C_{sp2\ BDY}$), 129.8 (C_E or C_F); 131.3, 132.8 ($C_{sp2\ BDY}$), 138.5 ($C_{sp2\ C60}$), 138.81 ($C_{sp2\ BDY}$), 138.83 ($C_{sp2\ C60}$), 139.5 ($C_{sp2\ C60}$), 140.1 ($C_{sp2\ BDY}$); [141.2, 142.0, 142.1, 142.4, 143.1, 143.19, 143.23, 143.25, 144.02, 144.04, 144.81, 144.84, 144.86, 145.0, 145.1, 145.2, 145.32, 145.34,

145.37, 145.42 ($C_{sp2\ C60}$)]; 153.8, 158.9 ($C_{sp2\ BDY}$); 163.5, 163.7 (C_f, C_h); 174.6, 176.9 (C_l). ^{19}F NMR (282 MHz, $CDCl_3$) δ -145.69 (q, J = 34.7 Hz); ^{11}B RMN (96 MHz, $CDCl_3$) δ 2.23 (t, J = 35.9 Hz); HRMS (ESI+) m/z calcd for $C_{100}H_{46}BF_2N_3O_7S$: 1482.3196 [M+H$^+$], found 1482.3147.

2.2 Spectra and Decay measurements

The UV/vis absorption spectra were implemented on a Varian Cary5000 spectrophotometer and corrected emission spectra were carried out on a Horiba FluoroMax+ in a right-angle configuration. The fluorescence quantum yields were measured relatively to Rhodamine 590 in ethanol Φ_F = 0.95 as a reference. Fluorescence intensity decays were measured by the TCSPC method with femtosecond laser excitation using a Spectra-Physics setup composed of a Titanium Sapphire laser (Tsunami, Spectra-Physics) pumpedby a doubled Nd:YVO4 laser (Millennia Xs, Spectra-Physics). Light pulses at 1000nm were selected by optoaccoustic crystals at a repetition rate of 4MHz, and a doubling crystal is used to reach the excitation wavelength of 500 nm. Fluorescence photons were detected (at 90°) through a monochromator using a Hamamatsu MCP R3809U photomultiplier, connected to a SPC-630 TCSPC module from Becker & Hickl. The fluorescence data were analyzed by a nonlinear least-squares method with the aid of Globals software package developed at the Laboratory of Fluorescence Dynamics at the University of Illinois, Urbana-Champaign.

2.3 Electrochemistry, Spectroelectrochemical absorption

2.3.1 Cyclic Voltammetry

BDP thioacetate **4**, fullerene **2**, and **BDP-C$_{60}$** Dyad were dissolved in anhydrous DCM or benzonitrile containing 0,1 M of n-Bu_4NPF_6 into a standard three-electrode cell under a nitrogen atmosphere. CV measurements were then undertaken with a potentiostat using a platinum disc electrode and a large platinum counter-electrode to obtain the potentials versus an Ag wire pseudo-

reference electrode. The latter was separated from the bulk solution using a capillary with frit. Potentials were calibrated versus ferrocene/ferrocenium.

2.3.2. Spectroelectrochemical Absorption

Spectra were recorded in a Varian Cary 5000 spectrophotometer using an OTTLE cell(51) composed of a Pt minigrid working electrode, a Pt wire counterelectrode, and an Ag wire pseudo-reference electrode connected to a potentiostat (CHInstruments 600). The sample was dissolved in dichloromethane containing 0.1 M hexafluorophosphate tetraethylammonium. Background was made on the cell filled with the electrolyte solution only.

2.4 Transient absorption measurement

2.4.1. Femtosecond transient absorption

Femtosecond UV-vis-NIR transient absorption spectra were collected on a commercially available system (Ultrafast Systems, Helios). The ultrafast laser system consists of a short-pulse titanium-sapphire oscillator (Mai-Tai, Spectra-Physics, 70 fs) followed by a high-energy titanium-sapphire regenerative amplifier (Spitfire Ace, Spectra-Physics, 100 fs). The 800 nm beam was split into two beams to generate: (1) pump (λ_{exc} = 527 nm) in the optical parametric amplifier (Topas Prime with NirUVis frequency mixer) and (2) probe pulses - white light continuum in UV-vis-NIR (330 – 1370 nm) range, using a CaF_2 plate (330 – 660 nm), sapphire (440 – 780 nm) and YAG crystal (830 – 1345 nm). The pump pulse energy was 0.4 μJ. The absorbance was close to 0.86 at the excitation wavelength in a 2 mm optical path quartz cell. The sample solution was stirred by a Teflon-coated bar; no significant degradation was observed. Before experimentation, the solution was saturated with argon. The entire set of pump-probe delay positions was repeated at least twice, to ensure data reproducibility. The transient absorption data were corrected for the chirp of the

white light continuum. The instruments response function (IRF) was about 200 fs (FWHM) in all experiments.

2.4.1. Nanosecond transient absorption

Nanosecond transient absorption measurements were measured on a home-built setup which has been described previously.[61] Briefly, the Nd:YAG pumped optical parametric oscillator (OPO) laser is used for sample excitation at 527nm with the energy of ~5mJ per pulse. The pump operates at 10Hz. After excitation, the sample is probed with a pulsed nanosecond white light continuum laser (LEUKOS) at a repetition rate of 20Hz. The probe beam is split into two arms, one for probing the sample and the other for reference in order to compensate for the pulse to pulse energy fluctuation. The probing arm after passing through the sample is coupled to a round to linear optical fibre bundle before being analyzed with a spectrograph SPEX 270 M (Jobin–Yvon). The detection of the dispersed white light is performed with an intensified CCD (ICCD) detector PIMAX 4 (Princeton Instrument). The transient absorption spectra can be calculated using the following formula:

$$\Delta OD = log_{10}\left(\frac{S_{ref}^{on}}{S_{ref}^{off}} \times \frac{S_{prob}^{off}}{S_{prob}^{on}}\right) \qquad (4)$$

Where S_{ref}^{on} and S_{ref}^{off} are reference spectra when the pump laser is on and off relatively, $S_{prob}^{off}$and S_{prob}^{on} are probe spectra when the pump laser is on and off relatively.

3. Results and discussion

3.1 Synthesis and Characterization

3.1.1. Synthesis

The synthesis of the BODIPY-C60 dyad (BDP-C60) from the fullerene and BODIPY building blocks 2 and 6, respectively, is outlined in Scheme 1. Briefly, the fullerene derivative 1 was prepared in five steps according to our previously published procedure.(50) The desired fullerene building block 2, functionalized with a maleimide moiety, was then prepared from 1 by performing a retro Diels–Alder reaction. For the preparation of the second building block (6), the synthesis starts with the preparation of the BODIPY derivative 3. This latter was obtained using a three-step one-pot approach. The kryptopyrrole was reacted with 4-(2-bromoethoxy)benzaldehyde in dry dichloromethane (DCM) and trifluoroacetic acid followed by p-chloranil oxidation and final treatment with boron trifluoride etherate in the presence of diisopropylethylamine. The BODIPY 3 was then reacted with potassium thioacetate in acetone to give the BODIPY 4. The desired BODIPY building block 6, functionalized by a thiol moiety, was thus prepared by reacting BODIPY 4 with potassium carbonate in a mixture of DCM and methanol under argon. The crude mixture was composed of the desired thiol derivative 6 along with the disulfide 5. This byproduct can be easily reduced by reacting the crude mixture with tributylphosphine in DCM under argon to give exclusively the BODIPY-thiol 6 in 82% yield. This derivative was purified by column chromatography and was used directly in the final step. Finally, the synthesis of the BODIPY-C60 dyad was realized by performing a Michael addition from the fullerene-maleimide 2 and the BODIPY-thiol 6 in DCM in the presence of triethylamine. The BODIPY-C60 dyad was isolated after chromatographic purification on a silica gel in high yield (87%).

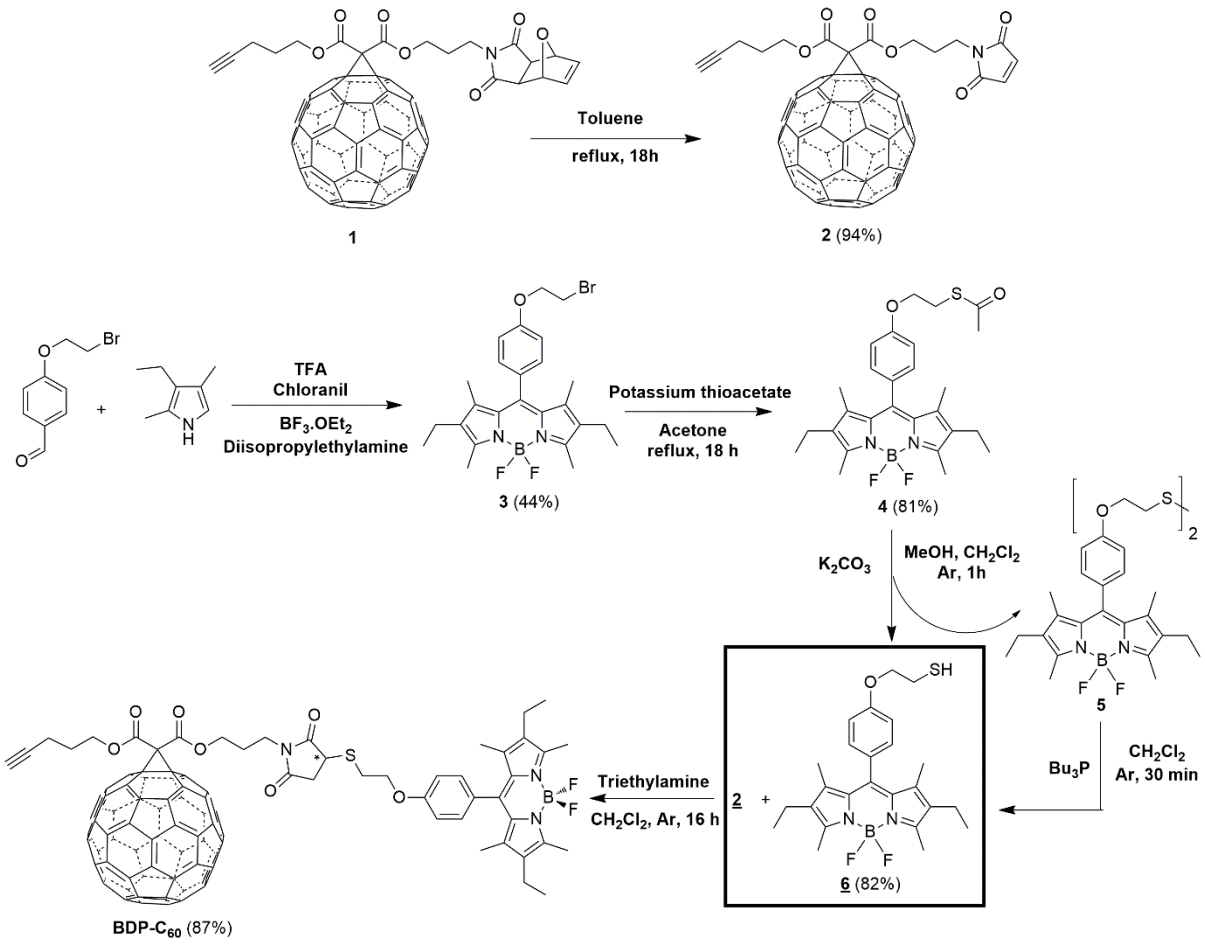

Scheme 1. Synthetic pathway for the preparation of the **BDP-C$_{60}$** Dyad.

3.1.2. NMR analysis

All the new compounds were fully characterized by NMR spectroscopy and by electrospray mass spectrometry; the recorded data were in accordance with the depicted structures (Figures S1–S7). Examination of the 1H NMR spectrum of the BODIPY-C60 dyad shows the signals corresponding to 1H of the fullerene (1H in blue) and BODIPY (1H in red) building blocks (Figure 2). Importantly, the formation of the thiol-maleimide adduct is confirmed by the disappearance of the maleimide protons at 6.75 ppm and the presence of a set of new signals in the 2.55–4.1 ppm region. These signals are attributed to the protons of the imide ring. 1H belonging to the chiral center (Hn) appears as a doublet of doublets at 4.04 ppm, while the methylenic protons (Hm) near this chiral

center are diastereotopic and display an AB pattern. Furthermore, the methylenic protons of the BODIPY moiety (HH) close to this chiral center are also diastereotopic leading to an AB pattern.

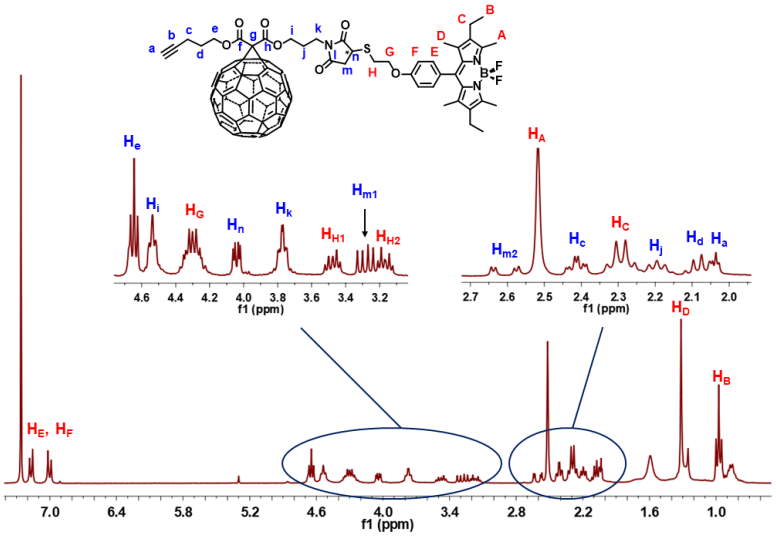

Figure 2. ^{1}H NMR spectrum recorded (300MHz, $CDCl_3$, 25°C) for the **BDP-C$_{60}$** Dyad.

3.2 Computational studies

3.2.1. Conformations of the BDP-C60 Dyad

The conformational search of the BODIPY-C60 dyad was carried out by theoretical calculations at the semi-empirical PM3 level. We first considered a set of two conformers for each enantiomer, in which the fullerene moiety and the thiol-maleimide bond are located on the same or opposite side with respect to the imide ring including asymmetric carbon. The geometries of these conformers, denoted S-(I, IV) and R-(II, III), were optimized at the PM3 level, and the most stable conformers (Figure 3) were used as initial points for further conformational study.

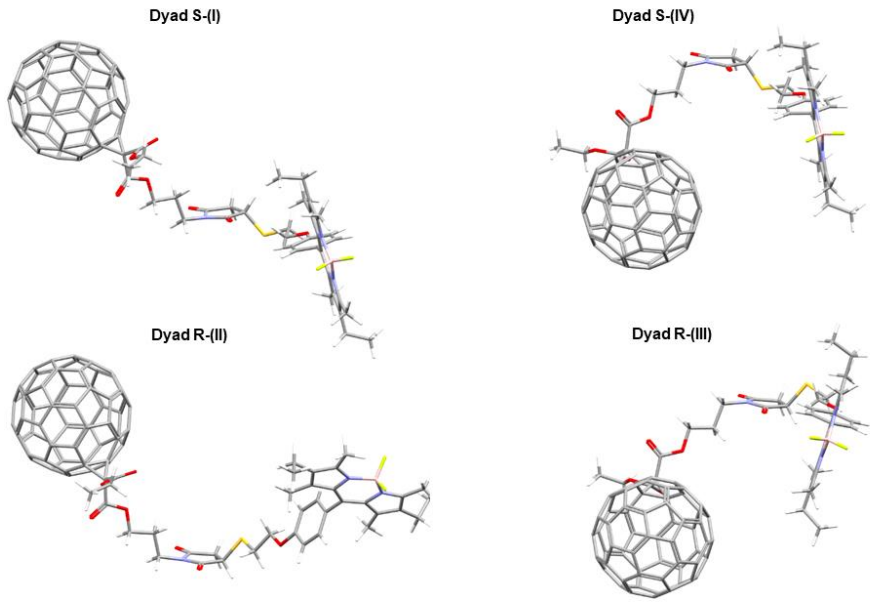

Figure 3. Conformers of the **BDP-C$_{60}$** optimized by semi-empirical calculations (PM3) used as initial points for further geometrical optimization. Alkynyl propyl group was substituted by an ethyl group for the computational study.

Then, the potential energy surfaces were scanned as a function of the OCN-CH2CH2 dihedral angle starting from R-(III) and S-(I) enantiomers to find out remarkable conformers when rotating the C60 moiety. Figure 4 and Figures S9 and S10 show the energy profiles of the dyad for both enantiomers. The R-(III) dyad gave two global minima, namely, R-(V) and R-(VI), which are close in energy and more stable in comparison to the starting conformer R-(III). These conformers R-(V) and R-(VI) are characterized by a folded and a stretched linear geometry, respectively, and separated with a rotational energy barrier close to 3.7 kcal·mol–1. The S-(I) dyad gave the same trend with new minima, namely, S-(VII) and S-(VIII), which are also characterized by a folded and a stretched linear geometry and a rotational energy barrier of 3.6 kcal·mol–1 (Figures S9 and S10). The results of the semi-empirical calculations show that there are at least two stable

conformations for the dyad in the R and S configurations. For both enantiomers, the rotational energy barrier between the two conformational minima is low. Hence, the dyad can easily adopt either a folded or a stretched linear geometry through the motion of the fullerene part like a windshield wiper (Figure 5).

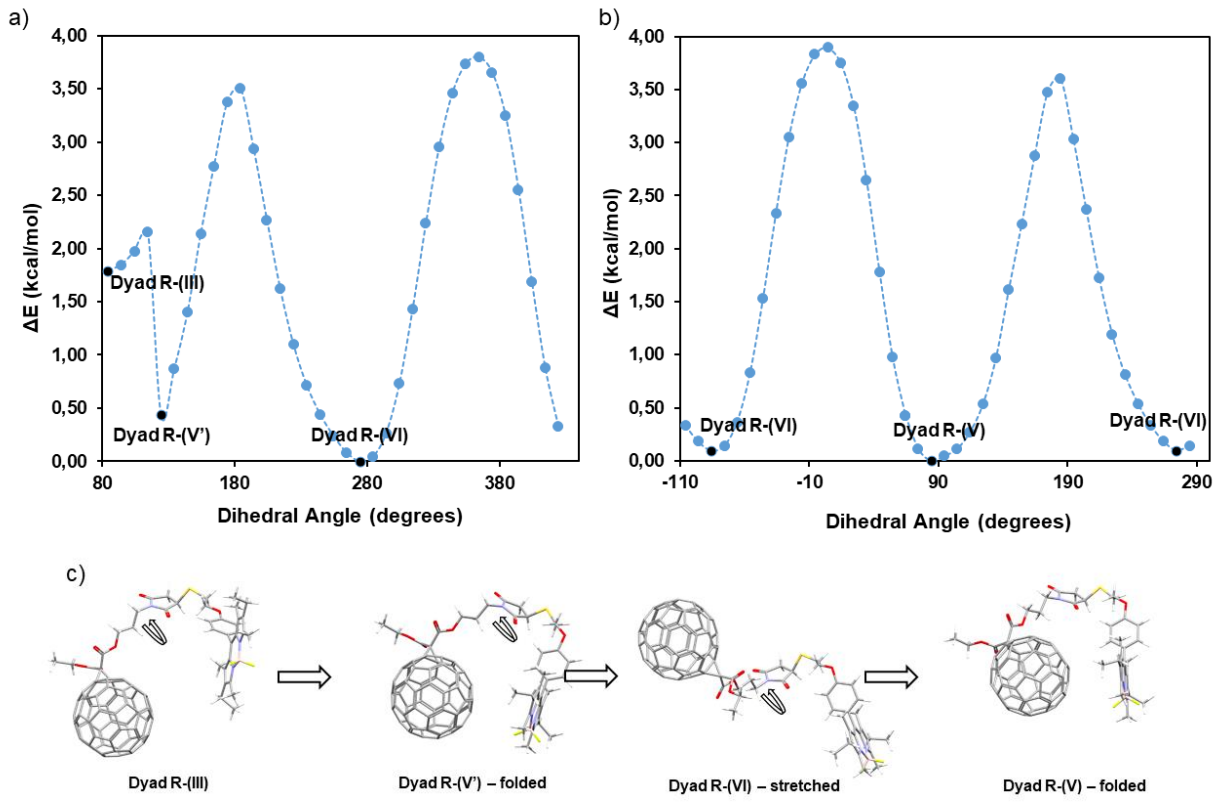

Figure 4. a and b) Calculated energy profileobtained by a relaxed scan aroundthe OCN-CH$_2$CH$_2$ dihedral angle for the (R) configuration. Energies are given relative to the minimum energy conformation. c) Theoretical structures of the different conformers, starting from the R-(III) conformer, including the two global minima R-(V) and R-(VI).

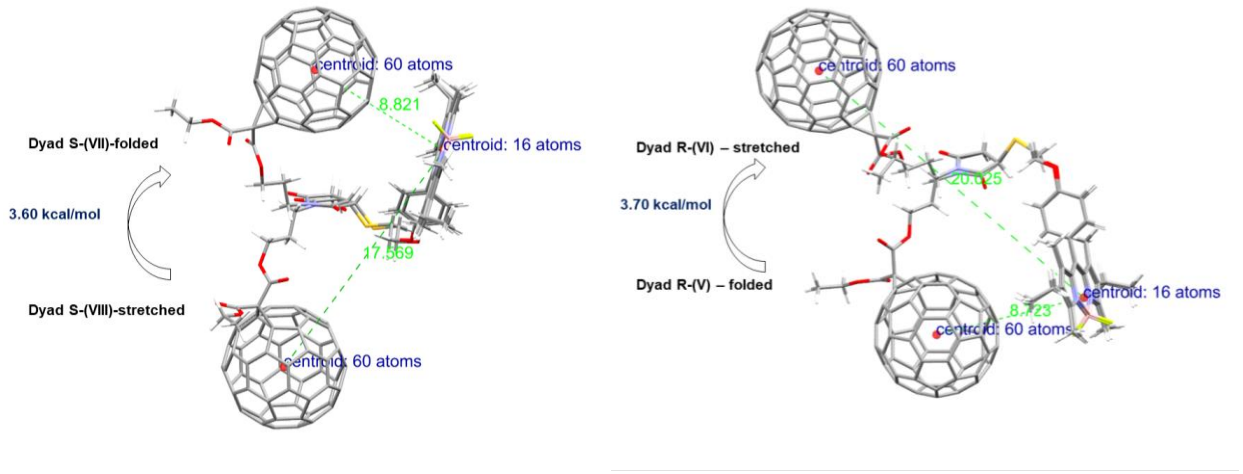

Figure 5. Rotational energy barrier between the folded and stretched linear geometry for both enantiomers along with the distances for each minimum-energy conformer.

In addition, we have determined the center-to-center distances between BODIPY and C60 for the most stable conformation. These distances are the same in the folded conformation for the (R) and (S) configurations, with a BODIPY-C60 distance of 8.8 Å, while in the stretched linear conformation, there are minor differences in the BODIPY-C60 distances with 20.0 and 17.5 Å for the (R) and (S) configurations, respectively (Figure 5). To summarize, due to the complexity of the conformation landscape of the dyad, we will focus on donor–acceptor distance to distinguish conformer 1 (R- or S-folded), conformer 2 (S-stretched), and conformer 3 (R-stretched) with BODIPY-C60 distances of 8.8, 17.5, and 20.0 Å, respectively.

3.2.2. Molecular Orbital Analysis

Finally, we also ran a single-point energy calculation using the long-range corrected cam-B3LYP hybrid functional and 6-311+g(d,p) basis set on the previously optimized conformations (S-(VII, VIII) and R-(V, VI), see Figure 5) of the BODIPY-C60 dyad to get a picture of the molecular orbitals (MO). As expected for the stretched linear geometry and whatever the configuration, MO are exclusively localized on the C60 or BODIPY moieties without

delocalization (Figures S12–S14). It is noteworthy that the LUMO is localized on the C60 electron acceptor while the HOMO is localized on the BODIPY electron donor unit. We have observed a similar trend for the folded geometry (Figure 6 and Figures S11–S13).

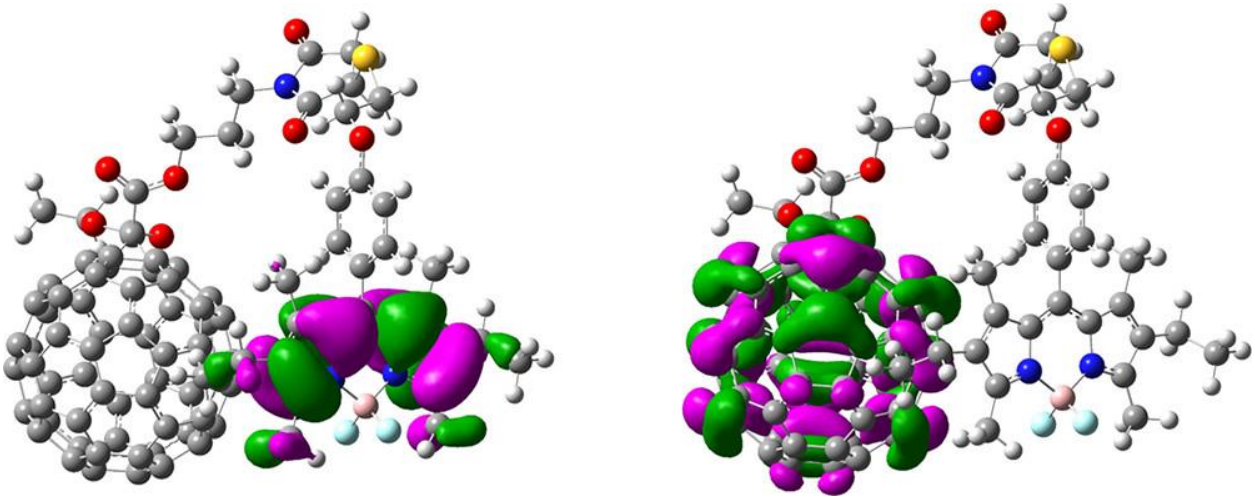

Figure 6. HOMO (left) and LUMO (right) for the folded R-(V) conformer.

3.3 Absorption and Fluorescence of the BODIPY-C60 Dyad

First of all, the absorption, emission, and coupling between the chromophores of the dyad have to be ascertained. To do so, the normalized absorption and fluorescence of the BODIPY-C60 dyad and BODIPY 4 in benzonitrile are compared in Figure 7.

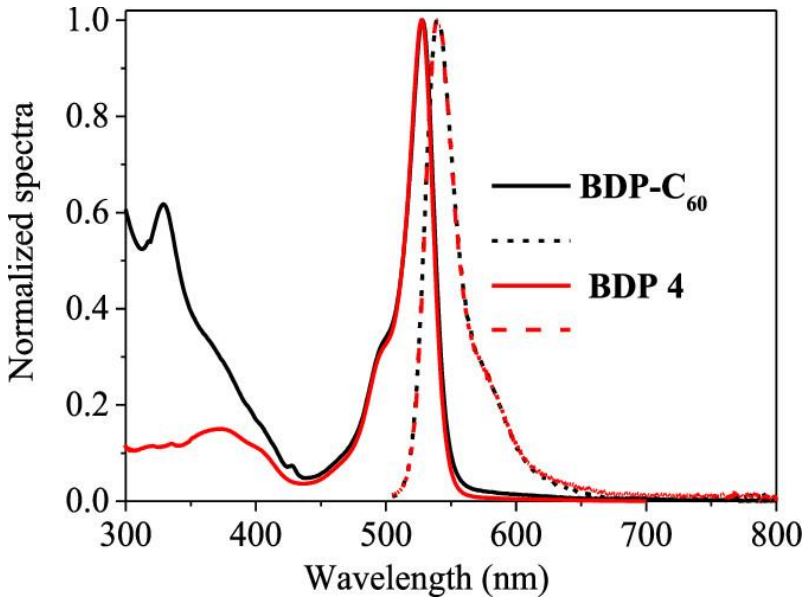

Figure 7. Normalized absorption (solid line) and fluorescence (dashed line) spectra in benzonitrile of the **BDP 4** ($1.3x10^{-6}$ M) and **BDP-C60** Dyad ($1.3x10^{-6}$ M) λ_{exc} = 510 nm. The normalized fluorescence spectra are almost identical for the two compounds.

First, the absorption of the BODIPY 4 shows the expected strong S0–S1 transition band at 527 nm and a higher energy S0–S2 transition band at 380 nm.(53) By comparison, the main absorption band of the BODIPY-C60 dyad is characteristic of this BODIPY fragment, while the expected contribution of the methanofullerene moiety is also present with a sharp band at 330 nm and a small band at 427 nm (Figure 7 and Figure S8).(54) It indicates that the C60 moiety does not affect the absorption spectra of the BODIPY moiety in the BODIPY-C60 dyad (for wavelengths longer than 440 nm), suggesting negligible ground-state interaction between BODIPY and C60 entities.

Upon excitation at 500 nm, the fluorescence spectrum of the BODIPY 4 in benzonitrile showed the well-known emission band of classical BODIPY peaking near 537 nm.(55) The normalized fluorescence spectra are almost identical for the BODIPY 4 and the BODIPY-C60 dyad, indicating that the BODIPY moiety is responsible for the dyad emission. The comparison of the fluorescence

spectra of the BODIPY 4 and BODIPY-C60 dyad recorded under the same conditions is shown in Figure 8a, while the photophysical parameters of these compounds are summarized in Table 1. As compared to the highly fluorescent BODIPY 4 compound with quantum yield ΦF = 0.73, the fluorescence of the BODIPY-C60 dyad is strongly quenched for more than 90%. We have therefore undertaken time-resolved fluorescence measurements using time-correlated single-photon counting (TCSPC) to gain some insights about this quenching (Figure 8b).

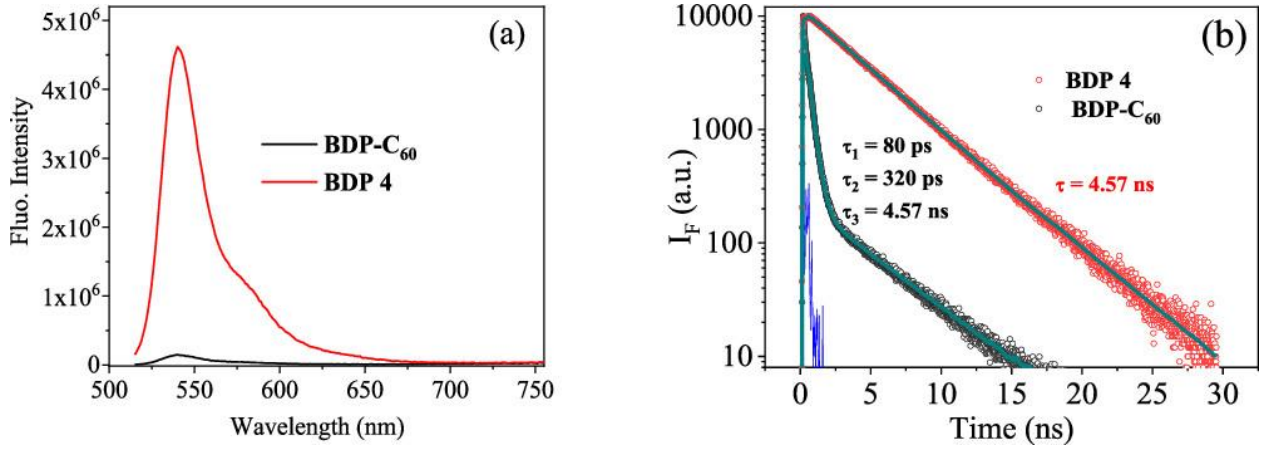

Figure 8. (a) Emission spectra and (b) fluorescence decay observed at 540 nm of the BODIPY-C60 dyad (BDP-C60) and BODIPY (BDP **4**) excited at 500 nm in benzonitrile (1.3×10^{-6} M). Blue line: instrument response function.

Table 1. Photophysical Parameters of BODIPY (BDP 4), C60 Building Block 2, and BODIPY-C60 Dyad in Benzonitrile[a]

compound	λ_{abs} (nm)	λ_{em} (nm)	ε_{max} (M^{-1} cm^{-1})	Φ_F	τ (ns)		k_r (10^8 s^{-1})	k_{nr} (10^8 s^{-1})
C_{60}**2**	330, 428	697b	3000b	0.0005b	1.50b	100%		
BDP **4**	380, 527	537c	74,500d	0.73	4.57 ± 0.04	100%	1.6 ± 0.1	0.6 ± 0.1
BDP-C_{60} dyad	330, 527	537c	77,500d	0.04	0.08 ± 0.04	41%	1.5 ± 0.1	36 ± 1
					0.32 ± 0.04	57%		
					4.57 ± 0.04	1%		

[a] Absorption λabs (nm) and emission λem (nm) maxima, molar absorption coefficient ε (M^{-1} cm^{-1}), fluorescence quantum yield Φ_F, fluorescence lifetimes τ (ns) with their amplitude contributions, radiative rate k_r (s^{-1}) and non-radiative rate k_{nr} (s^{-1}) constants.

[b] Ref (60).
[c] Excitation at 510 nm.
[d] At 527 nm.

First, the fluorescence decay of BODIPY 4 can be fitted with a single exponential function with a lifetime of 4.57 ns, which is characteristic of the BODIPY singlet excited state (1BDP*).(53) Reversely, the fluorescence of the BODIPY-C60 dyad has to be fitted with not less than three exponentials. A long-lived decay time (4.57 ns) similar to BODIPY 4 results has a minor 1% amplitude contribution and is easily attributed to the presence of "free BODIPY" because of the breaking of the thiol-maleimide bond, as already described in the literature.(56) In contrast, the two short lifetimes 80 and 320 ps with major amplitude contributions (41% and 57%, respectively) can be further demonstrated to relate with excited-state quenching, affecting two stretched conformers with different donor–acceptor distances in the dyad (see paragraph below).(57−59)

To assess such quenching, we deduce radiative and non-radiative rate constants related to the corresponding fluorescence quantum yield and decay according to $k_r = \Phi_F/\tau$ and $k_{nr} = 1/\tau - k_r$ (Table 1). Using the average lifetime obtained for the BODIPY-C60 dyad, we can notice that the radiative constant is very similar between the BODIPY-C60 dyad and the BODIPY 4, but significant enhancement of the non-radiative constant is observed for the BODIPY-C60 dyad. All these results strongly suggest that an interaction between the 1BDP* and C60 moiety in the BODIPY-C60 dyad exists through an electron transfer and/or energy transfer from 1BDP* to C60.

The ability of Förster resonance energy transfer (FRET) in the BODIPY-C60 dyad molecule can be estimated by using Förster theory. The Förster radius R0 (distance at which the energy transfer efficiency is 50%) is expressed according to eq 2(61)

$$R_0 = 0.2108 \times \left[n^{-4} \times \Phi_d \times \kappa^2 \times \int_0^\infty I_D(\lambda)\varepsilon_A(\lambda)\lambda^4 d\lambda \right]^{1/6} \text{(in Å)} \quad (2)$$

where n is the refractive index of the solvent (nbenzonitrile = 1.528), Φd is the emission quantum yield of the donor chromophore in the absence of the acceptor (Φd = 0.73 was used), κ2 is the orientation factor, and ID (λ) is the entire emission intensity normalized to unity. εA (λ) is the extinction coefficient of the acceptor. Considering a random distribution of dipole–dipole interaction (κ2 = 2/3), which is a rough approximation, the R0 value is assessed around 30 Å.

Using this value and the center-to-center distances of the BODIPY-C60 dyad determined from semi-empirical calculations, the rate of FRET for the different conformations could be estimated from eq 3, in which τD0 is the excited-state lifetime of the donor in the absence of the acceptor:

$$k_{FRET} = \frac{1}{\tau_D^0}\left[\frac{R_0}{R}\right]^6 \quad (3)$$

Among the different geometries (conformers 1–3), we decided to ignore the contribution of FRET for the folded conformers due to the short center-to-center distance in the BODIPY-C60 dyad molecule (8.8 Å). Indeed, the main relaxation pathways of the excited state are likely to be the ultrafast electron transfer (see section 3.5). Thus, we have considered the two stretched linear geometry conformers 2 and 3 with the long donor–acceptor distances (17.5 and 20.0 Å). Two approximate rate constants of excitation energy transfer ken1 = 5.5 × 109 s–1 and ken2 = 2.5 × 109 s–1 have been found, which correspond to typical lifetimes of 180 and 400 ps, respectively. These estimations corroborate nicely two short fluorescence lifetimes 80 and 320 ps, which were measured in TCSPC. Thus, we propose that the excited states of two conformers 2 and 3 are probably affected by FRET quenching.2.4 Electrochemical and spectroelectrochemical studies

3.4 Electrochemical and Spectroelectrochemical Studies

With anticipation, we expected some photoinduced electron transfer (PET) for the conformer 1 with a short distance between the donor and acceptor. Electrochemical studies are suitable to ascertain such statement.

3.4.1. Electrochemical Studies

To estimate the energies of charge-separated states formed by PET, the oxidation and reduction potentials of BODIPY (BDP 4), C602, and BODIPY-C60 dyad were determined by cyclic voltammetry (CV). All experiments were performed at room temperature in DCM and in benzonitrile containing tetra n-butylammonium hexafluorophosphate (0.1 M) as a supporting electrolyte. A platinum disk electrode was used as a working electrode, while a large platinum electrode was employed as the counterelectrode, and Ag wire was used as a pseudo-reference. Ferrocene (Fc) was added as an internal reference, and all the potentials were referenced relative to the Fc/Fc+ couple. The half-wave potentials for the BODIPY-C60 dyad along with those of the C602 and BODIPY 4 derivatives are reported in Table 2. The cyclic voltammograms of these compounds performed in DCM are presented in Figure 9. In the cathodic region, the BODIPY-C60 dyad displays two reversible reduction waves (Figure 9c). By comparison with the reduction potentials of those of the C602 (Figure 9a), these two waves are undoubtedly assigned to the two first reduction waves of C60. In the anodic region, the BODIPY-C60 dyad gives a reversible oxidation wave that is assigned to the oxidation of the BODIPY moiety by comparison with the oxidation potential of the pristine BODIPY 4 (Figure 9b). The cyclic voltammograms (Figure S15) were also recorded in benzonitrile to get the redox potentials, which will be used for the driving force calculations. The cyclic voltammograms are broader and less defined than those in DCM. However, the BODIPY-C60 dyad displays two first reversible reduction waves in the cathodic

region corresponding to the fullerene core, while in the anodic region, the oxidation wave is partially reversible and attributed to the BODIPY moiety.

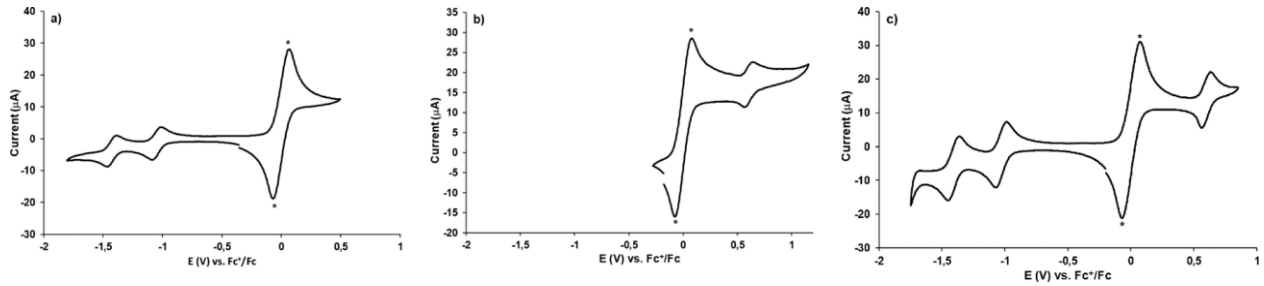

Figure 9. Cyclic voltammograms of a) **C_{60} 2**, b) **BDP 4**, and c) **BDP-C_{60}** Dyad in DCM. Oxidation and reduction waves of ferrocene, used as an internal standard, are denoted with an asterisk.

Table 2. Half-Wave Potentials (V) of **C_{60} 2**, **BDP 4**, and **BDP-C_{60}**[a] Dyad.

	DCM			**Benzonitrile**		
Compound	**$E^{1/2}{}_1$**	**$E^{1/2}{}_2$**	**$E^{1/2}{}_3$**	**$E^{1/2}{}_1$[b, c]**	**$E^{1/2}{}_2$[c]**	**$E^{1/2}{}_3$[c]**
fullerene **2**	-	-1.05	-1.43	-	-0.97	-1.37
BDP 4	0.60	-	-	0.59	-	-
BDP-C_{60} Dyad	0.60	-1.03	-1.41	0.59	-0.95	-1.38

[a] Versus ferrocene/ferrocenium. Experimental conditions: Compounds dissolved in anhydrous and oxygen-free DCM or benzonitrile solutions, 0,1M of *n*-Bu_4NPF_6, pseudo-reference electrode: Ag wire, working electrode: Pt, auxiliary electrode: Pt, scanning rate: 100mV.s^{-1}. [b] partially reversible. [C] broader and less defined redox waves.

Since the values of the half-wave potentials of the BODIPY-C60 dyad and the parents BODIPY and C60 are identical (Table 2), we can conclude that no significant electronic interactions are found for the BODIPY-C60 dyad in the ground state.

3.4.2. Driving force calculation (free energy changes)

Driving forces for the electron transfer were estimated based on redox potential measurements. The free-energy changes of the charge-separated state (ΔGCS) and charge recombination (ΔGCR) in the BODIPY-C60 dyad system were estimated by using the Rehm–Weller approach,(62) according to eqs 4 and 5

$$-\Delta G_{CR} = e\left[E_{ox}^{1/2} - E_{red}^{1/2}\right] - \Delta G_s \quad (4)$$

$$-\Delta G_{CS} = E_{0,0} - (-\Delta G_{CR}) \quad (5)$$

in which: $\Delta G_s = \frac{e^2}{4\pi\varepsilon_0}\left[\left(\frac{1}{2R_+} + \frac{1}{2R_-}\right)\Delta\left(\frac{1}{\varepsilon_R}\right) - \frac{1}{R_{cc}\varepsilon_R}\right]$ where ΔG_s is the solvation energy, E_{ox} is the half-wave potential for one-electron oxidation of the electron-donor unit, E_{red} is the half-wave potential for one-electron reduction of the electron acceptor unit, $E_{0,0}$ is the energy associated with the 0,0 optical transition (the corresponding midpoint of absorption and emission). The symbols ε_0 and ε_R refer to vacuum permittivity and dielectric constant of the employed solvent, respectively. The symbols R_+ and R_- refer to radii of the radical cation and radical anion species, respectively. R_{CC} is the center-to-center distance.

The calculated free-energy changes for the most stable conformations are given in Table 3. The values of ΔG_{CS} and ΔG_{CR} are negative in both DCM and benzonitrile solvents. These results show that electron transfer is thermodynamically favorable in both solvents.

Table 3. Free energy change of charge separation (ΔG_{CS}) and charge recombination (ΔG_{CR}) of the **BDP-C_{60}** Dyad in DCM and benzonitrile solvents.

	$-\Delta G_{CS}$ (eV)			**$-\Delta G_{CR}$ (eV)**		
Benzonitrile	0.78	0.77	0.77	1.55	1.56	1.56
DCM	0.72	0.70	0.70	1.61	1.62	1.63
R_{CC} (Å)	8.8	17.5	20.0	8.8	17.5	20.0

According to the Förster and the driving force calculations, both the energy and electron transfers are likely to occur within the BODIPY-C60 dyad molecule and might be both responsible for the BODIPY donor quenching.

3.4.3. UV-vis-NIR Spectroelectrochemistry of BODIPY 4 and C_{60} 2

In order to assign the absorption spectra of the charge-separated state in the dyad, spectroelectrochemistry experiments were carried out. The BODIPY-C60 dyad, pristine BODIPY 4, and C602 in DCM display entirely reversible oxidation and reduction processes. Thus, spectroelectrochemical absorptions were conducted in this solvent to locate the bands corresponding to the oxidized state of the BODIPY 4 and reduced state of the C602.

The spectroelectrochemical absorption spectra of the oxidized and reduced states of the pristine BODIPY 4 and C602 are shown in Figure 10. As the applied voltage gradually increases from 0.9 to 1.1 V, an increasing positive band at 407 nm is observed (Figure 10a). This band is characteristic of the oxidized state of the BODIPY 4.(35)

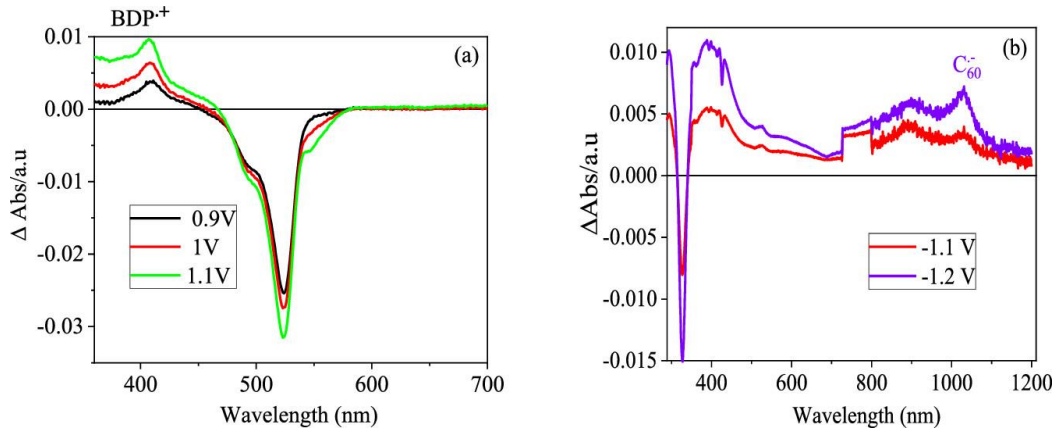

Figure 10. Differential absorption spectra relative to the neutral state of (a) the oxidized state of the BODIPY (BDP **4**) fragment (0.2 mM) and (b) the reduced state of the C60**2** fragment (0.3 mM) in dichloromethane under different potentials.

Figure 10b shows the NIR characteristic absorption bands of the reduced state of the C602 pristine under voltage applied (−1.2 V). The first reduced state of C60 (C60·–) has a sharp absorption band at 1035 nm.(24) The characteristic wavelength and profile of the reduced C60 absorption band are an ideal guide to support the distinction between energy transfer and electron transfer processes in femtosecond transient absorption experiments (see the next section).

3.5. Transient absorption studies

To depict the actual light-induced mechanisms standing on BODIPY-C60 in taking into account the complexity of the conformer landscape (conformers 1–3) and the previous photophysical and photochemical insights, namely, emission, FRET, and PET, transient absorption spectroscopy is the suitable technique. In consequence, transient absorption in the femtosecond and nanosecond regimes was carried out upon 527 nm selective photoexcitation of the BODIPY moiety in the BODIPY-C60 dyad in argon-saturated benzonitrile (Figures 11 and 12, respectively). For comparison, the TA spectra of the BODIPY 4 and C602 fragments in argon-saturated benzonitrile are presented in Figures S16 and S17. In the case of the femtosecond regime, both UV–vis and NIR detection regions were successively registered.

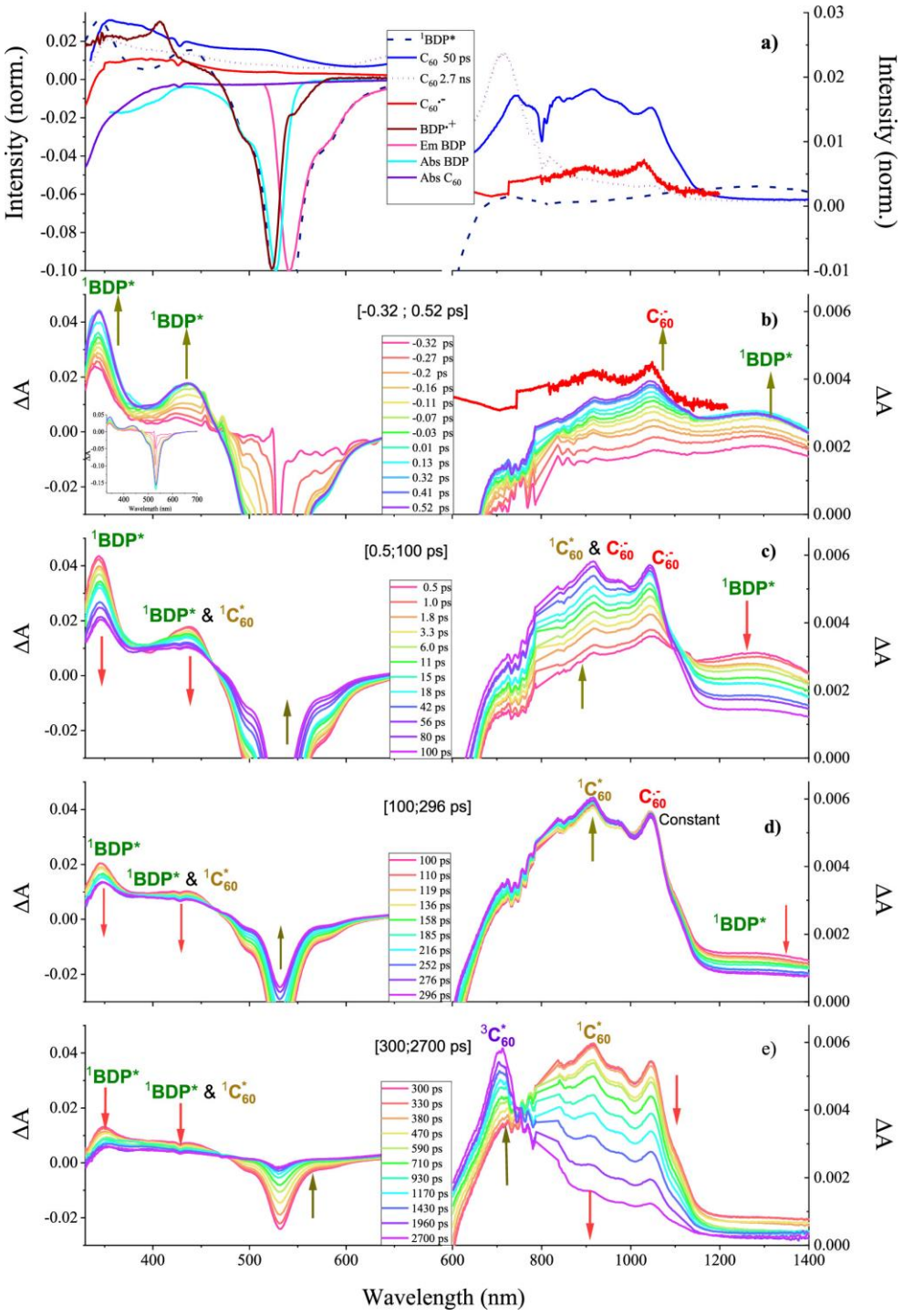

Figure 11. (a) Stationary spectra of BODIPY (BDP **4**), BDP $\mathbf{4}^{\bullet+}$, C60, and $C60^{\bullet-}$ and transient spectra of BODIPY (BDP **4**) and C60 in benzonitrile. (b–e) Femtosecond TA spectra at the indicated delay times of the BODIPY-C60 dyad (5.5×10^{-5} M) in argon-saturated benzonitrile (λ_{exc} = 527 nm). A difference spectrum after reduction of C60 by spectroelectrochemistry is also presented (red curve in b) for comparison. Abbreviations: singlet excited state of BODIPY (^{1}BDP*); singlet excited stated of C60 (^{1}C60*); triplet excited state of C60 (^{3}C60*); charge transfer state of C60 ($C60^{\bullet-}$).

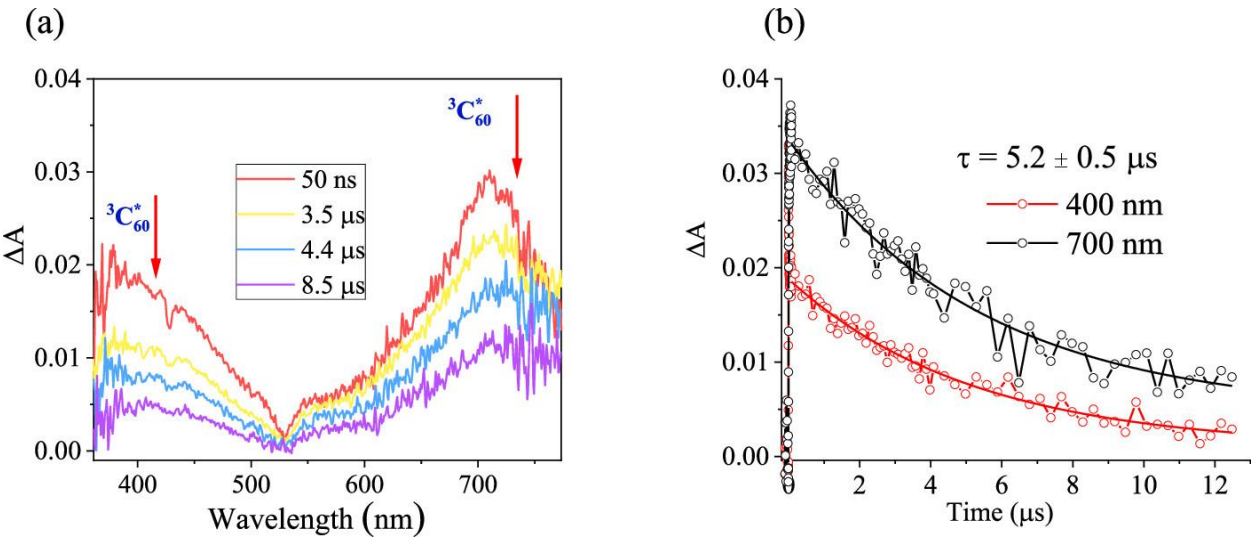

Figure 12. (a) Nanosecond TA spectra of the BODIPY-C60 dyad (5×10^{-6} M) in argon-saturated benzonitrile at the indicated delay times. (b) Kinetic traces probed at 400 and 700 nm (λ_{exc} = 527 nm).

3.5.1. Identifying transient species spectral signatures

Due to the complexity of the data, we will first review all the excited-state transient spectral signatures that will be chosen in order to perform global fitting analysis for the dyad considering both moieties separately. It is worth reminding that within the framework of both FRET and PET mechanisms between BODIPY and C60 moieties (apart from classical photophysics), the transient species of interest are the 1BDP*, 1C60*, 3C60*, BDP·+, and C60·– species (Figure 11a). First, as seen in Figure S16 and Figure 11a, the singlet excited state of the BODIPY 4, i.e., 1BDP*, is characterized by positive signatures at 340 and 450 nm together with a broad band in the NIR region with the maximum at 1278 nm. Additionally, the singlet excited state of the C602 shows wide absorption features in the whole visible and NIR region with a characteristic dip at 427 nm related to the ground-state bleaching. The contribution in the NIR region from 1000 to 1200 nm has been barely reported in the literature (Figure 11 and Figure S16).(63) Then, the triplet excited state of the C602 (3C60*) in argon-deaerated benzonitrile was found at 700 nm in nanosecond TA with the lifetime 6.6 μs (Figure S17). Finally, the spectral signature of BDP·+ and C60·– has been

investigated with a spectroelectrochemical setup (see above) with absorption bands at 407 and 1035 nm, respectively. Analysis will be quite complex since both $C60^{\cdot-}$ and 1C60* display a very similar absorption feature in the NIR. Both species present a peak at about 1030–1050 nm, and 1C60* shows an additional peak around 910 nm.

3.5.2. Photophysics and Charge Transfer of the Dyad

In Figure 11, for the sake of simplicity, the TA spectra of the BODIPY-C60 dyad are divided into four temporal windows distinguishing UV–vis [330–600 nm] and NIR regions [600–1400 nm] (eight panels in total). In parallel, we performed a fitting analysis choosing eight characteristic wavelengths with all the details given in Figures S18–S20 and Table S1. As just explained above, the choice of the wavelength has been made for the following reasons: the kinetic traces at 344, 427, and 1278 nm correspond to 1BDP*, at 700 nm correspond to the triplet excited state of C60 (3C60*), and at about 910 nm correspond to the main band of the singlet excited state of C60 (1C60*).(24,25,34) Negative absorption bands at 495 and 555 nm are assigned to the ground-state bleaching and stimulated emission, respectively. Finally, the kinetics of the charge transfer state can be followed at about 1045 nm corresponding to the first reduced state of C60 ($C60^{\cdot-}$), as shown in the spectroelectrochemical measurements. The global fitting procedure converged with five characteristic times: a very short time of <1 ps, 4 ps, 50 ps, 230 ps, and 1600 ps.

As seen in the first panels (time window, −0.3 to 0.5 ps), in parallel to the rise of 1BDP*, the clear rise of $C60^{\cdot-}$ is observed, providing evidence for an ultrafast charge transfer process from the Franck–Condon (FC) region (Figure 11b). To highlight such an effect, the absorption band of spectroelectrochemistry related to $C60^{\cdot-}$ has been superimposed. This ultrafast charge transfer process, with a probable rising time of several hundreds of femtoseconds, may correspond to conformer 1, with a shorter donor–acceptor distance of 8.8 Å, as illustrated in Figure 13.

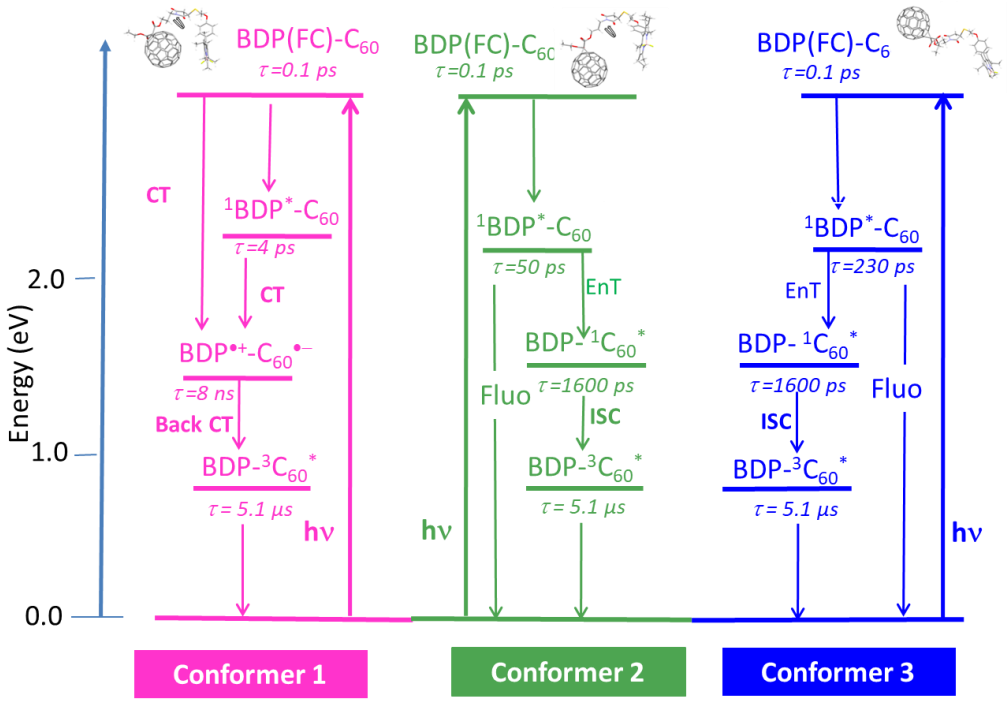

Figure 13. Energy level diagram presenting the photoinduced processes obtained following laser excitation (λ_{exc} = 527 nm) of the three conformers of the BODIPY-C60 dyad in benzonitrile. Abbreviations: FC, Frank–Condon; τ, lifetime; EnT, energy transfer; CT, charge transfer; CR, charge recombination; ISC, intersystem crossing. Dashed line: fluorescence and internal conversion; energies: ^{1}BDP* = 2.33 eV, ^{1}C60* = 1.79 eV,(24) ^{3}C60* = 1.50 eV.(24) Conformer 1: folded conformation (distance of 8.8 Å); conformers 2 and 3: stretched linear conformations (distances of 17.5 and 20.0 Å).

In the second temporal window ([0.5–100 ps]), an additional rise accompanied by narrowing of the C60·– band is observed with a characteristic time of 4 ps (Figure 11c). This process may be interpreted as a vibrational cooling(64) of C60·– initially formed with excess vibrational energy. Furthermore, the decay of 1BDP* is concomitant with a rise of both 1C60* (right panel) and bleaching band recovery (left panel) with a characteristic time of 50 ps. This time, being close to the 80 ps characteristic time found from the TCSPC experiment (see above), we can safely assign this process as energy transfer from 1BDP* to C60, which likely occur within the conformer 2. Similarly, the third panel (time windows, 100–300 ps) shows the decay of 1BDP* followed by ground-state recovery, with a characteristic time of 230 ps (related with 320 ps TCSPC, see above)

assigned as energy transfer in conformer 3. Moreover, we notice that the small features at around 1045 nm remain constant, in contrast with the increasing 910 nm large band of 1C60* (Figure 11d). This constant signal is likely to be explained by the simultaneous population of 1C60* and depopulation of $C60^{\cdot-}$ due to the charge recombination process. The time constants of the charge recombination and the first energy transfer are then approximatively estimated to be ∼50 ps.

For the final temporal window [300–2700 ps], the decay of the 1C60* band is noticed concomitantly with two other expected processes: (i) a ground-state recovery (bleaching band) and (ii) a rise of 3C60* transient band at 700 nm. This last observation gives evidence for the intersystem crossing (ISC) of 1C60* to 3C60* with a characteristic time of about 1.6 ns, which is exactly the same time as that reported by Palit et al.(65) To explore dynamics over the ns−μs time window, nanosecond transient experiments at an excitation wavelength of 527 nm were also performed on deaerated benzonitrile solution of the BODIPY-C60 dyad. Figure 12 shows the transient spectra and decay of the BODIPY-C60 dyad, with the absorption bands at 400 and 700 nm, which can be attributed to the absorption of 3C60* formed from the intersystem crossing process (see Figure S17). 3C60* decays with a time constant of 5.2 μs.

The overall transient spectroscopy data analysis together with the previous findings can be summarized with an energy diagram for the different photoinduced events of the BODIPY-C60 dyad in benzonitrile in Figure 13, taking into account the different conformers. The energy levels of the BODIPY-C60 dyad intermediates in benzonitrile are obtained from the excited-state energies and the redox potentials of the donor and acceptor units. The lifetime of the conformers 2 and 3 reported in the diagram was obtained from the time-resolved fluorescence measurements (Table 1). The time constants of the energy transfer process estimated from transient absorption kinetics were 50 and 230 ps for the conformers 2 and 3, respectively, which are consistent with

the fluorescence lifetime of these two conformers. Note that the contribution of energy transfer is more important for the conformer 2 with shorter fluorescence lifetime, indicating that the major contributions of 1C60* and consequently 3C60* were obtained from this conformer. The single exponential behavior of 3C60* observed in nanosecond transient absorption measurements is also in agreement with the fact that the excited state of C60 was principally formed from the conformer 2.

4. Conclusions

We have presented herein the synthesis and complete characterization, including semi-empirical and DFT calculations and electrochemical and photophysical studies, of a new molecular BODIPY-C60 dyad containing a BODIPY chromophore covalently linked to a fullerene acceptor. The geometries of at least three conformations of the BODIPY-C60 dyad are deduced from semi-empirical calculations with short and long acceptor–donor distances. The strong fluorescence quenching and the decrease in fluorescence lifetime in the BODIPY-C60 dyad are evidence of an interaction between 1BDP* and C60 moieties.

Transient absorption measurements were then conducted to decipher the overall excited-state mechanism in the dyad. Electrochemical studies allow the estimation of the energy of intermediate states, whereas spectroelectrochemistry measurements in the UV–vis–NIR region give the spectral signature of the acceptor in a reduced state, allowing assignment of the photoinduced charge-separated state. Transient absorption experiments demonstrate that both energy and electron transfers occur in this system. Ultrafast charge transfer from the Franck–Condon and 1BDP* states to the C60 moiety was attributed to the folded conformer with the BODIPY-C60 short distance. The energy transfer pathways come from the extended conformers. Such spectroscopic and electrochemical results have allowed a better understanding of all relaxation pathways of such a

flexible BODIPY-C60 dyad, which is a mandatory step before their immobilization on surfaces. Studies are currently in progress in order to immobilize the BODIPY-C60 dyad associated with helical peptides to develop photoelectrochemical devices.

ASSOCIATED CONTENT

Supporting Information. 1H, 13C, and 2D NMR spectra of the BODIPY-C60 dyad; energy profiles of the BODIPY-C60 dyad for the (S) configuration; main molecular orbitals (MO) of folded and extended conformers for the BODIPY-C60 dyad; normalized absorption spectrum of the fullerene 2 in benzonitrile; cyclic voltammograms of the fullerene 2, BODIPY 4, and BODIPY-C60 dyad in benzonitrile; femtosecond transient absorption spectra of the BODIPY 4 and fullerene 2 pristine in benzonitrile at the indicated delay times; nanosecond transient absorption spectra and kinetic traces of the fullerene 2 in air and in Ar-saturated benzonitrile; and femtosecond transient absorption kinetic traces, time constants, and decay associated spectra of the BODIPY-C60 dyad The supporting information is available free of charge via the internet at http://pubs.asc.org

AUTHOR INFORMATION

Corresponding Author

*E-mail: minh-huong.ha-thi@u-psud.fr.

*E-mail: emmanuel.allard@uvsq.fr

*E-mail: rachel.meallet-renault@u-psud.fr.

Present Addresses

Author Contributions

Funding Sources

Notes

ACKNOWLEDGMENT

This work was supported by the CNRS (PICS project n° 08198), the LabEx PALM ANR-10LABX-0039-PALM and CHARMMMAT ANR-11-LABX-0039. T.-T.T is grateful to the Vietnamese government for the scholarship (2016-2020)

ABBREVIATIONS

BDP, BODIPY; C_{60}, Fullerene; DFT, density functional theory; PET, photoinduced electron transfer; CV, cyclic voltammetry; DCM, dichloromethane; FRET, Föster energy transfer; NMR, Nuclear Magnetic Resonance; TCSPC, time-correlated single-photon counting; ET, electron transfer; EnT, energy transfer; CT, charge transfer; CR, charge recombination; ISC, intersystem crossing, k_T, rate constant for deactivation of triplet excited state of the C_{60}; TLC, thin layer chromatography.

REFERENCES

1 D'Souza, F.; Ito, O. *Coord. Chem. Rev.* **2005**, *249*, 1410-1422.
2 Guldi, D. M.; Rahman, A.; Sgobba, V.; Ehli, C. *Chem. Soc. Rev.* **2006**, *35*, 471-487.
3 Martín, N.; Sánchez, L.; Herranz, M. A.; Illescas, B.; Guldi, D. M. *Acc. Chem. Res.* **2007**, *40*, 1015-1024.
4 Fukuzumi, S. *Phys. Chem. Chem. Phys.* **2008**, *10*, 2283-2297.
5 Fukuzumi, S.; Kojima, T. *J. Mater. Chem.* **2008**, *18*, 1427-1439.
6 Balzani, V.; Credi, A.; Venturi, M. *ChemSusChem* **2008**, *1*, 26-58.
7 Gust, D.; Moore, T. A.; Moore, A. L. *Acc. Chem. Res.* **2009**, *42*, 1890-1898.
8 Wasielewski, M. R. *Acc. Chem. Res.* **2009**, *42*, 1910-1921.
9 González-Rodríguez, D.; Carbonell, E.; Guldi, D. M.; Torres, T. *Angew. Chem. Int. Ed.* **2009**, *48*, 8032-8036.
10 Fukuzumi, S.; Honda, T.; Ohkubo, K.; Kojima, T. *Dalton Trans.* **2009**, 3880-3889.
11 D'Souza, F.; Ito, O. *Chem. Commun.* **2009**, 4913-4928.
12 Guldi, D. M.; Illescas, B. M.; Atienza, C. M.; Wielopolski, M.; Martín, N. *Chem. Soc. Rev.* **2009**, *38*, 1587-1597.

13 Bottari, G.; de la Torre, G.; Guldi, D. M.; Torres, T. *Chem. Rev.* **2010**, *110*, 6788-6816.
14 D'Souza, F.; Sandanayaka, A. S. D.; Ito, O. *J. Phys. Chem. Lett.* **2010**, *1*, 2586-2593.
15 Gust, D.; Moore, T. A.; Moore, A. L. *Faraday Discuss.* **2012**, *155*, 9-26.
16 D'Souza, F.; Ito, O. *Chem. Soc. Rev.* **2012**, *41*, 86-96.
17 Dirian, K.; Herranz, M. A.; Katsukis, G.; Malig, J.; Rodríguez-Pérez, L.; Romero-Nieto, C.; Strauss, V.; Martín, N.; Guldi, D. M. *Chem. Sci.* **2013**, *4*, 4335-4353.
18 Espíldora, E.; Delgado, J. L.; Martín, N. *Isr. J. Chem.* **2014**, *54*, 429-439.
19 Joly, D.; Delgado, J. L.; Atienza, C.; Martín, N. in Light Harvesting Materials for Organics Electronics: Phtonics, Volume II, Scientific Foundations, Technology and Applications (Eds: Andrews, D. L.), Wiley, **2015**.
20 Rudolf, M.; Kirner, S. V.; Guldi, D. M. *Chem. Soc. Rev.* **2016**, *45*, 612-630.
21 Zieleniewska, A.; Lodermeyer, F.; Roth, A.; Guldi, D. M. *Chem. Soc. Rev.* **2018**, *47*, 702-714.
22 Ponseca, Jr., C. S.; Chábera, P.; Uhlig, J.; Persson, P.; Sundström, V. *Chem. Rev.* **2017**, *117*, 10940-11024.
23 Guldi, D. M.; Prato, M. *Acc. Chem. Res.* **2000**, *33*, 695-703.
24 Ziessel, R.; Allen, B. D. ; Rewinska, D. B.; Harriman, A. *Chem. Eur. J.* **2009**, *15*, 7382-7393.
25 Wijesinghe, C. A.; El-Khouly, M. E.; Blakemore, J. D.; Zandler, M. E.; Fukuzumi, S.; D'Souza, F. *Chem. Commun.* **2010**, *46*, 3301-3303.
26 Liu, J.-Y.; El-Khouly, M. E.; Fukuzumi, S.; Ng, D. P. P. *Chem. Asian J.* **2011**, *6*, 174-179.
27 Yang, P.; Wu, W.; Zhao, J.; Huang, D.; Yi, X. *J. Mater. Chem.* **2012**, *22*, 20273-20283.
28 Liu, J.-Y.; El-Khouly, M. E.; Fukuzumi, S.; Ng, D. K. P. *ChemPhysChem* **2012**, *13*, 2030-2036.
29 El-Khouly, M. E.; Fukuzumi, S.; D'Souza, F. *ChemPhysChem* **2014**, *15*, 30-47.
30 Bandi, V.; Das, S. K.; Awuah, S. G.; You, Y.; D'Souza, F. *J. Am. Chem. Soc.* **2014**, *136*, 7571-7574.
31 Bandi, V.; Gobeze, H. B. ; D'Souza, F. *Chem. Eur. J.* **2015**, *21*, 11483-11494.
32 Shao, S.; Gobeze, H. B.; Karr, P. A.; D'Souza, F. *Chem. Eur. J.* **2015**, *21*, 16005-16016.
33 Bandi, V.; Gobeze, H. B.; Lakshmi, V.; Ravikanth, M.; D'Souza, F. *J. Phys. Chem. C* **2015**, *119*, 8095-8102.
34 Iagatti, A.; Cupellini, L.; Biagiotti, G.; Caprasecca, S.; Fedeli, S.; Lapini, A.; Ussano, E.; Foggi, P.; Marcaccio, M.; Mennucci, B.; Di Donato, M. *J. Phys. Chem. C* **2016**, *120*, 16526-16536.
35 Obondi, C. O.; Lim, G. N. ; Karr, P. A.; Nesterov, V. N.; D'Souza, F. *Phys. Chem. Chem. Phys.* **2016**, *18*, 18187-18200.
36 Liu, J.-Y.; Hou, X.-N.; Tian, Y.; Jiang, L.; Deng, S.; Röder, B.; Ermilov, E. A. *RSC Adv.* **2016**, *6*, 57293-57305.
37 Ünlü, H.; Okutan, E. *Dyes and Pigments* **2017**, *142*, 340-349.
38 Shao, S.; Thomas, M. B.; Park, K. H.; Mahaffey, Z.; Kim, D.; D'Souza, F. *Chem. Commun.* **2018**, *54*, 54-57.
39 Cabrera-Espinoza, A.; Insuasty, B.; Ortiz, A. *Journal of Luminescence* **2018**, *194*, 729-738.
40 Bañuelos, J. *Chem. Rec.* **2016**, *16*, 335-348.
41 Yamada, H.; Imahori, H.; Nishimura, Y.; Yamazaki, I.; Ahn, T. K.; Kim, S. K.; Kim; D.; Fukuzumi, S. *J. Am. Chem. Soc.* **2003**, *125*, 9129-9139.
42 Imahori, H.; Fukuzumi, S. *Adv. Funct. Mater.* **2004**, *14*, 525-536.
43 Amdursky, N. *ChemPlusChem* **2015**, *80*, 1075-1095
44 Venanzi, M.; Gatto, E.; Formaggio, F.; Toniolo; C. *J. Pept. Sci.* **2017**, *23*, 104-116.
45 Gatto, E.; Venanzi, M. *Isr. J. Chem.* **2015**, *55*, 671-681.
46 Constant, C.; Albert, S.; Zivic, N.; Baczko, K.; Fensterbank, H.; Allard, E. *Tetrahedron* **2014**, *70*, 3023-3029.
47 Fensterbank, H.; Baczko, K.; Constant, C.; Idttalbe, N.; Bourdreux, F.; Vallée, A.; Goncalves, A.-M.; Méallet-Renault, R.; Clavier, G.; Wright, K. ; Allard, E. *J. Org. Chem.* **2016**, *81*, 8222-8233.
48 Nasrallah, H.; Rabah, J.; Bui-Thi-Tuyet, V.; Baczko, K.; Fensterbank, H.; Bourdreux, F.; Goncalves, A.-M.; Declerck, V.; Boujday, S.; Humblot, V.; Wright, K.; Vallée, A.; Allard, E. *New. J. Chem.* **2018**, *42*, 19423-19432.

49 Chaudhuri, T.; Mula, S.; Chattopadhyay, S.; Banerjee, M. *Spectrochimica Acta Part A* **2010**, *75*, 739-744.
50 Guldi, D.M.; Hungerbuhler, H.; Carmichael, I.; Asmus, K.-D.; Maggini, M. *J. Phys. Chem. A* **2000**, *104*, 8601-8608.
51 Baffreau, J.; Leroy-Lhez, S.; Anh, N.V.; Williams, R.M.; Hudhomme, P. *Chem. Eur. J.* **2008**, *14*, 4974-4992.
52 Fazio, M.A.; Durandin, A.; Tkachenko, N.V.; Niemi, M.; Lemmetyinen, H.; Schuster, D.I. *Chem. Eur. J.* **2009**, ***15***, 7698-7706.
53 Guldi, D.M.; Giacalone, F.; de la Torre, G.; Segura, J.L.; Martín, N. *Chem. Eur. J.* **2005**, *11*, 7199-7210.
54 Bell, T.D.M.; Ghiggino, K.P.; Haynes, A.; Langford, S.J.; Woodward, C.P. *J. Porphyr. Phthalocyanines* 2007, **11**, 455-462.
55 Ravasco, J. M. J. M.; Faustino, H.; Trindade, A.; Gois, P. M. *Chem. Eur. J.* **2019**, *25*, 43-59.

56 Reference See O'Shea.
57 Philbin, M.L. *Mod. Cast.* **1996**, *86*, 30-33.
58 Főrster, T. Discuss. Faraday Soc. **1959**, *27*, 7 -17.
59 Wijesinghe, C.A.; El-Khouly, M.E.; Subbaiyan, N.K.; Supur, M.; Zandler, M.E.; Ohkubo, K.; Fukuzumi, S.; D'Souza, F. *Chem. Eur. J.* **2011**, *17*, 3147-3156.
60 Gampp, H.; Maeder, M.; Meyer, C.J.; Zuberbühler, A.D. *Talanta* **1985**, *32*, 95-101.
61 Mendes Marinho, S.; Ha-Thi, M.H.; Pham, V.T.; Quaranta, A.; Pino, T.; Lefumeux, C.; Chamaillé, T.; Leibl, W.; Aukauloo, A. *Angew. Chemie - Int. Ed.* **2017**, *56*, 15936-15940.